JOURNAL OF THERMOPHYSICS AND HEAT TRANSFER
Vol. 6, No. 4, Oct.–Dec. 1992

Transient Behavior of Heat Pipes with Thermal Energy Storage Under Reversed-Pulsed Heat Loads

Ming-Jr Chang* and Louis C. Chow†
University of Kentucky, Lexington, Kentucky 40506
and
Won Soon Chang‡ and Micheal Morgan§
Aero Propulsion and Power Laboratory, Wright-Patterson Air Force Base, Ohio 45433

A novel design of a high-temperature axially grooved heat pipe (HP) which incorporates thermal energy storage (TES) to mitigate reversed-pulsed heat loads applied at the condenser is presented. Liquid sodium, which is used to remove the heat released by a power generator, circulates through an HP/TES cooling device, where the heat is rejected into space. The transient behavior of the HP/TES system is simulated using a three-dimensional alternating-direction-implicit (ADI) finite difference numerical model. A phase-change material (PCM) encapsulated in cylindrical containers is used for thermal energy storage. The transient response of three different HP/TES configurations was compared 1) a heat pipe with a large empty cylinder installed in the vapor core, 2) a heat pipe with a large PCM cylinder, and 3) a heat pipe with six small PCM cylinders. From the numerical results it was found that the PCM is very effective in mitigating the adverse effects of reversed-pulsed heat loads.

Nomenclature

C = heat capacitance
c = specific heat
D_h = hydraulic diameter of vapor flow
f = vapor friction coefficient or f factor
H = enthalpy
$\bar{h}$ = average convection heat transfer coefficient
k = thermal conductivity
l_c = length of condensation region
Ma = Mach number
$\dot{m}$ = axial local vapor mass flow rate
P = vapor pressure
$\dot{Q}$ = total heat rate
q = heat flux
Re = axial Reynolds number of vapor flow
Re_w = radial Reynolds number of vapor flow
r, θ, z = space coordinates
Ste = Stefan number of phase change material
T = temperature
t = time
U = mean axial vapor velocity
v = radial vapor velocity
α = thermal diffusivity
γ = ratio of specific heats
Δ = finite difference operator
δ^2 = central difference operator
ρ = density
σ = Stefan-Boltzmann constant
τ = dimensionless time

Subscripts
c = condenser
e = evaporator
g = power generator
hp = heat pipe
i,j,k = nodal point indices in r, θ and z directions
l = liquid state
loop = liquid sodium loop
rev = reverse
s = solid state

Superscript
n = time index

Received March 6, 1991; presented as Paper 91-1404 at the AIAA 26th Thermophysics Conference, Honolulu, HI, June 24–26, 1991; revision received Sept. 20, 1991; accepted for publication Oct. 5, 1991.

*Graduate student, Mechanical Engineering.
†Professor, Mechanical Engineering. Senior Member AIAA.
‡Senior Research Scientist.
§Engineer.

Introduction

FUTURE space missions will involve thermal transport devices with the ability to handle reversed-pulsed heat loads. Figure 1 shows a schematic diagram of the cooling system for a power generator. A certain amount of heat is constantly released by the power generator and removed by the liquid sodium loop. The sodium loop circulates through the heat pipe/thermal energy storage (HP/TES) cooling device, where the heat is rejected into space. Under normal conditions the system is operated at steady state. Suddenly an incident heat pulse strikes the condenser section of the HP/TES cooling device. Under such a severe condition, not only the heat released by the power generator cannot be

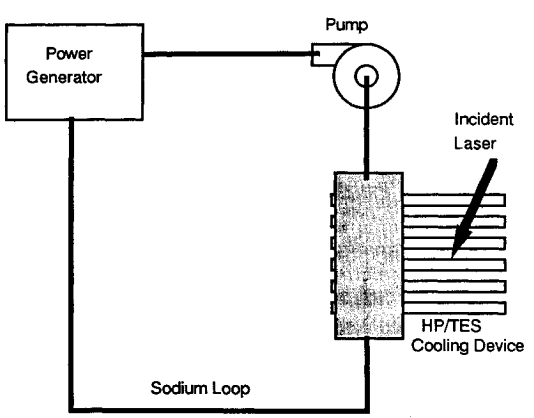

Fig. 1 Schematic diagram of the cooling system for a power generator.

removed, but also the reversed-pulsed heat loads caused by the incident heat pulse will be reversely transferred into the liquid sodium loop. The system temperature will increase dramatically under these conditions. Incorporation of TES into heat pipe rejection systems can be a promising method to mitigate the reversed-pulsed heat loads applied at the condenser. The transient response of different heat pipes [with or without phase-charge material (PCM)] under the reversed-pulsed heat loads are investigated in this article. Tilton et al.[1] and El-Genk et al.[2] have examined the transient response of a heat pipe under external thermal loading at the condenser. However, they did not provide a mitigation technique to handle these reversed-pulsed heat loads. The HP/TES configuration was first studied by Chang et al.,[3] and they showed that the TES with PCM is very effective in mitigating the adverse effect of pulsed heat loads applied at the evaporator.

The transient numerical model used in this paper was mainly developed by Chang et al.[3] An improved three-dimensional ADI finite difference method presented by Chang et al.[4] was used to model the heat conduction through the wall and wick, including the liquid in the grooves. The vapor flow was modeled by Bowman[5] using a quasisteady one-dimensional friction coefficient. Bowman made a very important conclusion that the vapor flow can be modeled as a quasisteady process, since the response time of the vapor dynamics is very short compared to the heat transfer response time of the heat pipe wall and wick. He also suggested that it is adequate to treat the vapor flow as one-dimensional. In the numerical solution of heat conduction problems with phase change (Stefan's problem), Pham[6,7] suggested a simple method which combines enthalpy and heat capacity methods. He concluded that his method is very accurate and much faster than other methods. However, Pham's method has a singularity problem in finding the equivalent specific heat. In this research we adopted the best features of Pham's method and made some modifications to improve on its weak points. Compared with analytical solutions this modified method for melting and solidification was found to have very good accuracy, without the singularity problem of Pham's method.

We applied this numerical model (described below) to a heat pipe of 1.0 m in length. A stainless-steel grooved heat pipe using sodium as its working fluid was modeled. Three different HP/TES configurations, as shown in Fig. 2, were tested with several types of reversed-pulsed heat loads. A simple lumped-heat-capacity model was also used to predict the transient behavior of the heat pipe without PCM. Compared with the results from the finite difference solution, it was found that the lumped-heat-capacity model can predict the average heat pipe temperature and the heat flow input/output at the evaporator and condenser very well for the heat pipe without PCM.

Numerical Model

We used the lumped-heat-capacity method to simulate the liquid sodium loop system. The heat-pipe-evaporator wall surface temperature was assumed to be equal to the sodium loop temperature, because the heat transfer coefficient is very high. The heat transfer through the heat pipe wall and wick (including the liquid in the grooves) was modeled as three-dimensional in the radial, angular, and axial directions. We assumed that the heat transfer through the wick and working fluid is by conduction only, since the liquid flow velocity is very low and the liquid thermal conductivity is very high. Also it was assumed that the grooves are nearly filled with liquid. This is a good assumption for high-temperature heat pipes under normal operation without dryout, because the thermal resistance of a liquid metal is much smaller than that of the heat pipe wall. The top lands of the groove structure in the evaporator section were assumed adiabatic because no evaporation occurs. The thermal resistance of the condensed liquid on the top lands of the groove structure in the condenser section is very small compared to the thermal resistance of the solid wall and was neglected. The liquid/vapor interface temperature was assumed equal to the local vapor temperature, because the thermal resistances due to evaporation and condensation are very small. The vapor flow was modeled by using a quasisteady, one-dimensional friction coefficient model. Since the thermal resistance of the condensed liquid on the TES is much smaller than that of the phase-change material, the surface temperature of the TES is assumed to be equal to the vapor temperature at the same axial location. Hence if the PCM is encapsulated in a cylindrical container, only a two-dimensional analysis is needed to calculate the temperature and heat transfer within the PCM because of angular symmetry.

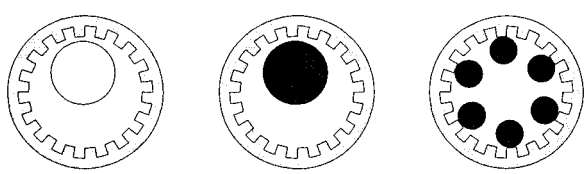

Fig. 2 Three different HP/TES configurations.

Pipe Wall and Wicks

The improved three-dimensional ADI finite difference method[4] was used to model the heat conduction through the wall and wick, including the liquid in the grooves. The advantage of the ADI method is that only tridiagonal matrices need to be solved. However, the conventional three-dimensional ADI method is conditionally stable, and very small time steps are required to ensure convergence and stability. Since a very small Δr (about 0.3 mm) is needed due to the slender geometry of the heat pipe, only a very small Δt (about 0.001 s) can be used with the conventional ADI method. The conventional ADI method was modified by introducing an f factor ($0 < f < 1$). This modification allows the time step to be increased by about two orders of magnitude without significantly compromising the accuracy of the numerical solution.

After the three-dimensional finite difference equations of the conventional ADI method with cylindrical coordinates are modified by an f factor, they become the following equations:

$$\frac{1}{\alpha}\frac{T^{n+1/3}_{i,j,k} - T^{n}_{i,j,k}}{\Delta t/3} = (3 - 2f)\delta_r^2 T^{n+1/3}_{i,j,k} + f\delta_\theta^2 T^{n}_{i,j,k} + f\delta_z^2 T^{n}_{i,j,k} \quad (1)$$

$$\frac{1}{\alpha}\frac{T^{n+2/3}_{i,j,k} - T^{n+1/3}_{i,j,k}}{\Delta t/3} = f\delta_r^2 T^{n+1/3}_{i,j,k} + (3 - 2f)\delta_\theta^2 T^{n+2/3}_{i,j,k} + f\delta_z^2 T^{n+1/3}_{i,j,k} \quad (2)$$

$$\frac{1}{\alpha}\frac{T^{n+1}_{i,j,k} - T^{n+2/3}_{i,j,k}}{\Delta t/3} = f\delta_r^2 T^{n+2/3}_{i,j,k} + f\delta_\theta^2 T^{n+2/3}_{i,j,k} + (3 - 2f)\delta_z^2 T^{n+1}_{i,j,k} \quad (3)$$

It was shown[4] that the time-step limit for the conventional ADI method can now be increased by a factor of $1/f$ by using this new ADI method. The computational results showed that this modification allows the time-step limit to be increased by two orders of magnitude with $f = 0.01$, while the solutions still remain stable with very high accuracy. The thermal diffusivity α used for Eqs. (1–3) is determined based on the local properties and temperature at each nodal point.

Melting and Solidification of PCM

In the numerical solution of heat conduction problems with phase change (Stefan's problem) by finite differences, enthalpy methods or heat capacity methods can be used. The former methods require either an explicit procedure which may lead to convergence problems, or iteration at each time

step if an implicit procedure is used. The latter methods are subject to the problem of jumping the latent heat peak, necessitating the use of very small time steps to avoid underprediction of the phase-change time. Recently Hsiao[8] proposed a new finite difference method for Stefan's problems. In his scheme the equivalent heat capacity at a node is a function of the temperature at that node and all the surrounding nodes. Hsiao concluded that his method can avoid the problem of jumping the latent heat peak and allows the use of a relatively large time step. Hsiao's method was tested, but a large energy balance error was found. Pham[6,7] suggested a simple method which includes features from both the enthalpy and heat capacity methods. Comparing this method with other existing methods for test problems with exact solutions, Pham pointed out that most of the methods agree to within 0.2% with analytical results, except for the Hsiao's method which yielded results up to 22% in error. The low accuracy of the Hsiao's method could be due to its ambiguous theoretical basis. Pham also concluded that his method is much faster than other approaches.

Pham's method can be used in conjunction with a two-dimensional ADI scheme using the following procedures:

1) At the start of each time step, the enthalpy change ΔH^* in each control volume is estimated from the heat fluxes through its control surfaces. The heat fluxes through the control surfaces are determined from the temperature gradient between the central node and its immediate neighbor nodes at the previous time step.

2) Since the enthalpy is a continuous function of the temperature for the phase-change material, we can determine an estimated new temperature $T^*_{i,k}$ from the following equation:

$$T^*_{i,k} = f_T[f_H(T^n_{i,k}) + \Delta H^*_{i,k}] \tag{4}$$

where $T^n_{i,k}$ is the nodal temperature at the previous time step, and f_T and f_H are the temperature and enthalpy functions, respectively.

3) When the estimated new temperature $T^*_{i,k}$ is known, the equivalent specific heat of each node can be obtained from the equation

$$c^*_{i,k} = \frac{\Delta H^*}{T^*_{i,k} - T^n_{i,k}} \tag{5}$$

4) With the equivalent specific heat $c^*_{i,k}$ known, we can use the two-dimensional ADI method to find the new nodal temperature $T^{n+1}_{i,k}$.

One of the good features of Pham's method is that it estimates the new temperature from the estimated enthalpy change to avoid the problem of jumping the latent heat peak. Another good feature of Pham's method is that its theoretical basis is clear. However, Pham's method has a singularity problem in finding the equivalent specific heat in step 2. If there is no enthalpy change at a particular node, the estimated new temperature $T^*_{i,k}$ will be equal to the previous temperature $T^n_{i,k}$. Then we are not able to find the equivalent specific heat from Eq. (5). Fortunately we have found a way around this problem. If the melting temperature is T_m and the latent heat effect is over a $2\Delta T_m$ interval, let $H_1 = f_H(T_m - \Delta T_m)$, $H_2 = f_H(T_m + \Delta T_m)$ and $H^{n+1}_{i,k} = H^n_{i,k} + \Delta H^*$. We redefine the equivalent specific heat in Eq. (5) as follows:

$$c^*_{i,k} = \begin{cases} c_s & \text{if } H^n_{i,k},\ H^{n+1}_{i,k} < H_1 \\ (H_2 - H_1)/(2\Delta T_m) & \text{if } H_1 < H^n_{i,k},\ H^{n+1}_{i,k} < H_2 \\ c_l & \text{if } H^n_{i,k},\ H^{n+1}_{i,k} > H_2 \\ \Delta H^*/(T^*_{i,k} - T^n_{i,k}) & \text{if } H^n_{i,k} < H_1 < H^{n+1}_{i,k} \\ & \text{or } H^n_{i,k} < H_2 < H^{n+1}_{i,k} \\ & \text{or } H^n_{i,k} > H_1 > H^{n+1}_{i,k} \\ & \text{or } H^n_{i,k} > H_2 > H^{n+1}_{i,k} \end{cases} \tag{6}$$

where c_s and c_l are the specific heats for solid state and liquid state.

After the modification, Eq. (5) now is used when only one of $H^n_{i,k}$ or $H^{n+1}_{i,k}$ falls between H_1 and H_2. In other words, Eq. (5) will only be used when ΔH^* is not equal to zero. Compared with analytical solutions, this modified method for melting and solidification was found to have very good accuracy and does not have the singularity problem of Pham's method.[4]

One-Dimensional Vapor Flow Model

The vapor flow was modeled by using a quasisteady, one-dimensional friction coefficient developed by Bowman.[5] In the evaporation region, mass blowing causes a slight steepening in the velocity gradients at the pipe wall, leading to an increase in the friction coefficient. Bowman pointed out that the favorable pressure gradient in the mass blowing region influences the flow to remain laminar, even for very large axial Reynolds numbers up to 10^6. In the condenser region, where there is mass removal and an adverse pressure gradient, the flow was found to stay laminar at axial Reynolds numbers around 12×10^3. In this article the vapor flow was always assumed to be laminar, because the maximum axial Reynolds numbers are always less than 12×10^3. The correlation of the vapor friction coefficient for laminar flow given by Bowman can be expressed as

$$f = 16/Re(1.2337 - 0.2337\, e^{0.0363 Re_w}) e^{6Ma^2/5} \tag{7}$$

where Ma is the Mach number based on the local mean axial velocity U, Re_w is the radial Reynolds number, and Re is the axial Reynolds number defined as

$$Re_w = \rho v D_h/\mu, \quad Re = \rho U D_h/\mu$$

In these expression, ρ is the vapor flow density, μ is vapor dynamic viscosity, v is the radial velocity at the wall, and D_h is the hydraulic diameter of the vapor core.

The vapor flow was assumed to be compressible, one-dimensional, and quasisteady. The governing equations for such a flow can be expressed in terms of influence coefficients as presented by Shapiro[9]

$$\frac{dMa^2}{Ma^2} = F_{f,a} 4f \frac{dz}{D_h} + F_{\dot m,a} \frac{d\dot m}{\dot m} \tag{8}$$

with the two influence coefficients given by

$$F_{f,a} = \frac{4Ma^2\,[1 + (\gamma - 1)Ma^2/2]}{1 - Ma^2} \tag{9}$$

$$F_{\dot m,a} = \frac{2[1 + \gamma Ma^2]\,[1 + (\gamma - 1)Ma^2/2]}{1 - Ma^2} \tag{10}$$

where f is the friction coefficient defined earlier by Eq. (7), γ is the ratio of specific heats, z is the axial coordinate, and $\dot m$ is the mass flow rate.

For the friction solution, a second expression is needed to relate the change in total pressure (P_0) to the change in mass flow rate and to the friction coefficient. From Shapiro[9]

$$\frac{dP_0}{P_0} = F_{f,b} 4f \frac{dz}{D_h} + F_{\dot m,b} \frac{d\dot m}{\dot m} \tag{11}$$

where

$$F_{f,b} = -\gamma Ma^2/2 \tag{12}$$

$$F_{\dot m,b} = -\gamma Ma^2 \tag{13}$$

To calculate the pressure and temperature variations in the vapor flow, we need to know the evaporation and condensation rates. However, these rates depend on the vapor temperature and heat pipe wall temperature distributions. This

means that the vapor pressure and temperature variations are intrinsically coupled to the evaporation and condensation rates. In the present model the evaporation and condensation rates are coupled to the vapor temperature and pressure in an explicit manner, so that no iterations are required. However, we still have to guess the vapor temperature at the evaporator end to calculate the vapor temperature distribution. The vapor temperature at the evaporator end can be estimated based on the following assumption: Since the vapor density is very small, we can assume that the heat absorbed by the vapor itself is negligible compared to the evaporation and condensation rates. In other words, at every time step, the evaporation rate and the condensation rate are equal.

Results and Discussions

We applied the present numerical model to a heat pipe with 18 grooves, using sodium as the working fluid. The material for the heat pipe container was type 316 stainless steel, and the total length of the heat pipe was 1.0 m with the evaporator, condenser, and adiabatic sections having lengths of 0.3 m, 0.3 m, and 0.4 m, respectively. The heat pipe outside diameter was 1.9 cm (3/4 in.), and the inside diameter was 1.4 cm. Heat was transferred from the sodium loop to the heat pipe evaporator section by forced convection and was removed at the condenser by radiative heat transfer to an ambient maintained at 0 K. The emissivity of the condenser wall surface was assumed equal to unity. Lithium hydride, which has a latent heat of 2.58×10^6 J/kg and a melting temperature of 956 K, was used as the PCM.

The liquid sodium loop temperature was predicted by the following equation based on the lumped-heat-capacity method:

$$C_{\text{loop}}(\Delta T_{\text{loop}}/\Delta t) = \dot{Q}_g - \dot{Q}_e \qquad (14)$$

Since this study was focused on only a single heat pipe unit, it should be noticed that C_{loop} and $\dot{Q}_g$ in Eq. (14) are the total sodium loop heat capacitance and the heat rate released from the power generator, respectively, divided by the total number of heat pipes in the system. The heat rate released from the power generator $\dot{Q}_g$ is always positive and remains constant. $\dot{Q}_e$ is defined as the heat rate transferred from the sodium loop to the heat pipe and is evaluated from the temperature gradient in the heat pipe wall. It can become negative when a reversed heat load is applied. If liquid sodium with velocity 1 m/s is circulating through the heat pipe, a very high surface heat transfer coefficient (about 5×10^4 W/m^2 K) can be obtained. Since the heat transfer coefficient is so high, we assumed that the heat pipe evaporator wall surface temperature is equal to the sodium loop temperature.

For the numerical modeling of the heat pipe wall and wick, eight nodes were used in the radial direction and 40 in the axial direction. Only four nodes were needed in the angular direction for a groove unit. The transient response of three different HP/TES configurations was compared 1) a heat pipe with a large empty cylinder installed in the vapor core, 2) a heat pipe with a large PCM cylinder, and 3) a heat pipe with six small PCM cylinders. The radii of the large cylinder and small cylinder are 0.4 and 0.163 cm, respectively. These sizes were chosen so that the large PCM cylinder holds the same total amount of PCM as the six small PCM cylinders. The vapor hydraulic diameters are about 0.82 cm for the heat pipe with one large PCM cylinder and about 0.75 cm for the one with six small PCM cylinders. For numerical modeling of the PCM, 40 nodes in the radial direction were chosen for the large PCM cylinder and 16 nodes were used for the small one. A phase transition temperature interval $2\Delta T_m = 10$ K was assumed, and a time step, $\Delta t = 0.1$ s, was used for all the examples in this article.

Figure 3 shows the transient response of three HP/TES configurations with $C_{\text{loop}} = 1000$ J/K when a reversed heat load is suddenly applied at the condenser. Prior to $t = 10$ s, the three heat pipes all are operating at steady-state conditions

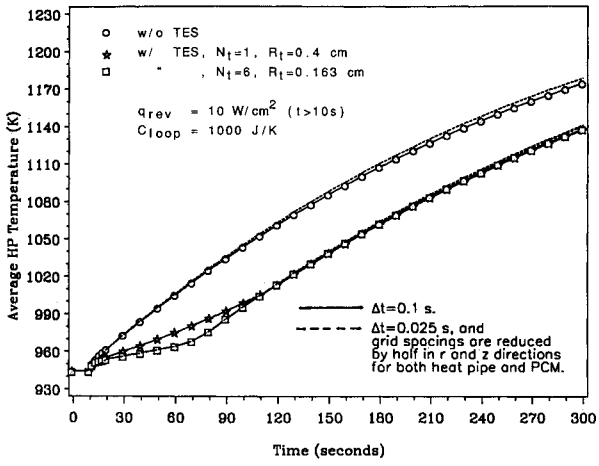

Fig. 3 Transient response of heat pipes with $C_{\text{loop}} = 10{,}000$ J/K under a reversed-pulsed heat load.

with the temperature of the sodium loop maintained at 950 K. Under this steady-state condition, the total heat rate transferred from the sodium loop $\dot{Q}_e$ is about 0.78 kW (for an average surface heat flux of about 4.3 W/cm^2) and is equal to the total heat rate removed at the condenser by radiation transfer $\dot{Q}_c$. The average heat pipe temperature is about 945 K. A heat transfer rate of 0.78 kW is continuously released from the power generator to the sodium loop throughout the entire operating period. After $t = 10$ s, a reversed heat load of $q_{\text{rev}} = 10$ W/cm^2 is suddenly applied to the condenser. As we can see, the temperature of the heat pipe without PCM increases rapidly. On the other hand, the temperatures of the other two heat pipes with PCM also increase rapidly immediately after the reversed heat load is applied. But the rapid temperature increase is arrested after the PCM reaches its melting temperature and starts to melt. It can also be seen that the temperature increase during the melting process with six small PCM cylinders is slower than with one large PCM cylinder. This slower temperature rise occurs because the total surface area of the six small PCM cylinders available for heat transfer is larger, and the heat conduction path is shorter compared to the case with one large PCM cylinder. However the six small PCM cylinders will be completely melted earlier at about $t = 80$ s compared to $t = 110$ s for the one large PCM cylinder. After the PCM is completely melted, both PCM heat pipes undergo rapid temperature increases until they reach a new steady-state condition.

As we mentioned earlier, Bowman[5] verified experimentally that the response time of the vapor dynamics is much shorter than the heat transfer response time of the heat pipe wall and wick. In other words, the transient response of a heat pipe is mainly controlled by the heat conduction through the heat pipe wall and wick. Thus an accurate heat conduction model is important in order to obtain high-accuracy solutions. The new three-dimensional ADI method developed by the authors[4] was used to model the heat conduction in the wall and wick. It was shown that this new ADI method is faster and has much higher accuracy than other popular methods for transient three-dimensional heat conduction problems. One can see from Ref. 4 that this new ADI method has very high accuracy with error less than 1% as long as the stability and accuracy conditions from Eqs. (26) and (31) in Ref. 4 are satisfied. Due to the complexity of the present heat pipe problem, we are not able to predict the error of the numerical solutions accurately, because no analytical solution is available. However, in order to retain high accuracy, the time step and grid spacings used in this research were chosen to satisfy the stability and accuracy conditions in Ref. 4. Under these conditions, the error of the present numerical solutions should be only a few percent. To further validate the numerical solutions, we applied the numerical model to the same problem

depicted in Fig. 3 by using a smaller time step $\Delta t = 0.025$ s and reducing the grid spacings in the r and z directions by half for both the heat pipe and PCM. As we can see from Fig. 3, the solutions remain almost the same with smaller values of the time step and grid spacings. Also, we have checked the total energy balance and found the error is less than 1% at each time step.

Figure 4 shows the variations of heat input $\dot{Q}_e$ and heat output $\dot{Q}_c$ of three different HP/TES configurations with $C_{\text{loop}} = 1000$ J/K under a reversed heat load applied at the condenser. The total heat rate transferred from the sodium loop to the heat pipe evaporator $\dot{Q}_e$ can be determined by knowing the temperature gradient inside the wall along the evaporator. The total heat rate removed from the condenser $\dot{Q}_c$ is the summation of the heat removed by radiation and the reversed heat load. Prior to $t = 10$ s, all three heat pipes are operating at steady state with a heat input of $\dot{Q}_e = 0.78$ kW equal to a heat output of $\dot{Q}_c = 0.78$ kW. After a reversed heat load $q_{\text{rev}} = 10$ W/cm^2 is applied at $t = 10$ s, the heat outputs at the condensers of the three heat pipes all become negative, indicating that there are external heat loads being added at the condensers. However, these heat outputs all begin to increase due to greater heat removal by radiation at the higher condenser wall temperatures. The variation of heat output is similar to that of the heat pipe temperature, because the heat output depends strongly on the condenser wall surface temperature.

The heat input variation is a strong function of the sodium loop heat capacitance C_{loop}. After the reversed heat load is applied, the heat input of the heat pipe without PCM decreases very rapidly in the first 10 s and is reversed to negative. After $t = 20$ s, the heat input begins to increase, because the heat output increases, and the reversed heat flow effect becomes less and less. The heat inputs of the other two heat pipes with PCM also decrease rapidly right after the reversed heat loads are applied. After the PCM starts to melt at about $t = 15$ s, the heat inputs increase very rapidly. This rapid increase occurs because a lot of reversed heat is absorbed by the PCM, and the heat pipe temperature increase becomes very slow. However, the heat inputs decrease slightly during later stages of the melting proces since the capability of the PCM to absorb the reversed heat load is declining. The heat inputs for the two heat pipes with PCM drop again and reverse to negative after the PCM is completely melted, because the heat pipe temperature starts to increase rapidly. It can also be seen that the heat input of the heat pipe with six small PCM cylinders is higher than that of the one with a single large PCM cylinder during the melting process. The greater heat input occurs because the temperature of the heat pipe with six small PCM cylinders is lower. The three different HP/TES configurations all tend to reach to a new steady-state temperature with same original heat input and heat output equal to 0.78 kW.

Figure 5 shows the transient response of three different HP/TES configurations with $C_{\text{loop}} = 10{,}000$ J/K under a reversed heat load suddenly applied at the condenser. Before $t = 10$ s, all three heat pipes are operating at steady-state conditions, as we discussed in the earlier case. After $t = 10$ s, a reversed heat load of $q_{\text{rev}} = 10$ W/cm^2 is applied at the condenser. As we can see, the temperature increase of all three HP/TES configurations is very slow. Because of its high heat capacitance, the sodium loop acts like a huge heat sink which can absorb most of the reversed heat loads and arrest the heat pipe temperature increase. It is clear that with such a high sodium loop heat capacitance, installation of PCM to mitigate the reversed heat loads is unnecessary.

Figure 6 shows the variations of heat input and heat output of three different HP/TES configurations with $C_{\text{loop}} = 10{,}000$ J/K under a reversed heat load applied at the condenser. Compared with the results shown in Fig. 4 for the case with $C_{\text{loop}} = 1000$ J/K, the heat inputs of all three heat pipes decrease very rapidly and all are reversed to negative after the reversed heat load is applied. With such a high sodium loop heat capacitance, the loop itself behaves like a massive heat sink and can easily absorb the reversed heat loads. The heat inputs of the two heat pipes with PCM are reversed less than the one without PCM after the reversed heat loads are applied. However, they immediately drop again after the PCM is completely melted.

We also applied the lumped-heat-capacity model to predict the transient behavior of the heat pipe without PCM. The

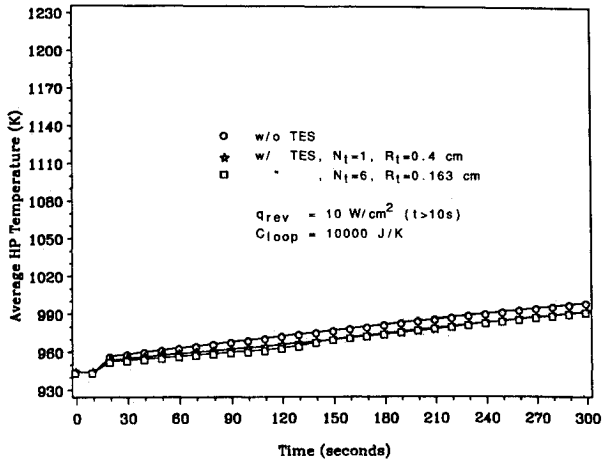

Fig. 5 Transient response of heat pipes with $C_{\text{loop}} = 1000$ J/K under a reversed-pulsed heat load.

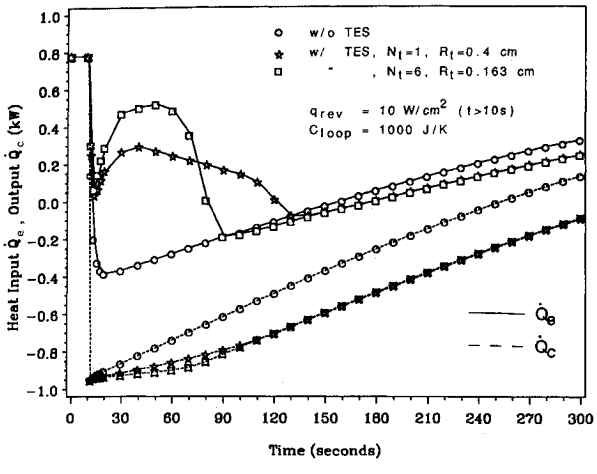

Fig. 4 Variations of heat input and heat output of heat pipes with $C_{\text{loop}} = 10{,}000$ J/K under a reversed-pulsed heat load.

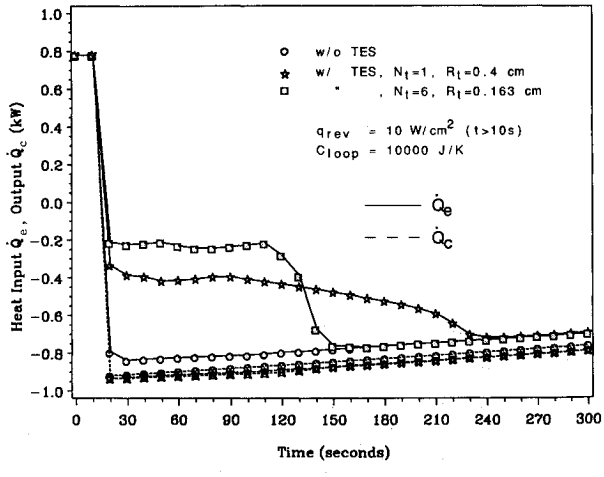

Fig. 6 Variations of heat input and heat output of heat pipes with $C_{\text{loop}} = 1000$ J/K under a reversed-pulsed heat load.

average heat pipe temperature was predicted by the following equation:

$$C_{hp}(\Delta T_{hp}/\Delta t) = \dot{Q}_e - \dot{Q}_c \tag{15}$$

where $\dot{Q}_e = \bar{h}A_e(T_{\text{loop}} - T_{hp})$ and $\dot{Q}_c = A_c(\sigma T_{hp}^4 - q_{\text{rev}})$.

Equation (15) is coupled with Eq. (14) to calculate the sodium loop and heat pipe temperatures. For the lumped-heat-capacity model, an average surface heat transfer coefficient between the liquid sodium loop and the heat pipe evaporator $\bar{h} = 5 \times 10^4$ W/m^{2}K was assumed. The heat capacitance of the heat pipe C_{hp} is about 540 J/K. Figure 7 shows the transient response of the heat pipe without PCM under reversed heat loads as predicted by the lumped-heat-capacity model. It can be seen that the results from the lumped model have very good agreement with those from the finite difference method. The lumped model can predict the average heat pipe temperature and the heat flow input/output at the evaporator and condenser very well for the heat pipe without PCM. The heat pipe temperature predicted by the lumped model is about 10 K lower than that predicted by the finite difference method over the entire time period analyzed. This discrepancy is a consequence of overestimating the heat removed from the condenser by radiation using the average heat pipe temperature as the condenser wall surface temperature.

Figure 8 shows the axial variation of vapor mass flow rate for two different HP/TES configurations with $C_{\text{loop}} = 1000$ J/K. At $t = 10$ s, both heat pipes are operating at steady-state conditions with forward heat loads applied at the evaporators. All the vapor mass flow rates are positive along the two units. The vapor mass flow rates increase at the evaporator section, remain almost constant across the adiabatic section, and then decrease in the condenser section. As can be seen from Fig. 6, the vapor flow of the heat pipe without PCM is totally reversed at $t = 60$ s as both heat input and heat output are negative. For the heat pipe with six small PCM cylinders, the vapor flow becomes two separate flows with opposite directions as the heat input is positive and the heat output is negative. Evaporation occurs at both evaporator and condenser sections, while the vapor condenses in the adiabatic section and on the outside surfaces of the PCM containers. As shown in Fig. 8, the vapor mass flow rate is positive only at the evaporator section and in part of the adiabatic section. It is negative for the rest of the heat pipe. One should also note that the vapor mass flow rate at the adiabatic section of the heat pipe changes more rapidly with six small PCM cylinders than it does when no PCM is present. This is because a considerable amount of vapor condenses on the outside surfaces of the PCM containers during the melting process.

Figures 9a and 9b show the axial variation of vapor pressure and temperature for two different HP/TES configurations with $C_{\text{loop}} = 1000$ J/K. At $t = 10$ s, both heat pipes are operating under steady-state conditions. The variation of the vapor pressure for both heat pipes is almost the same, because there is not much difference in heat pipe temperature and vapor mass flow rate. At $t = 60$ s, both heat pipes have a higher vapor pressure at the condenser end, because the vapor flows are reversed. The vapor pressure drops along both heat pipes at $t = 60$ s are much less than they were at $t = 10$ s. For the heat pipe without PCM, the smaller pressure drop is mainly

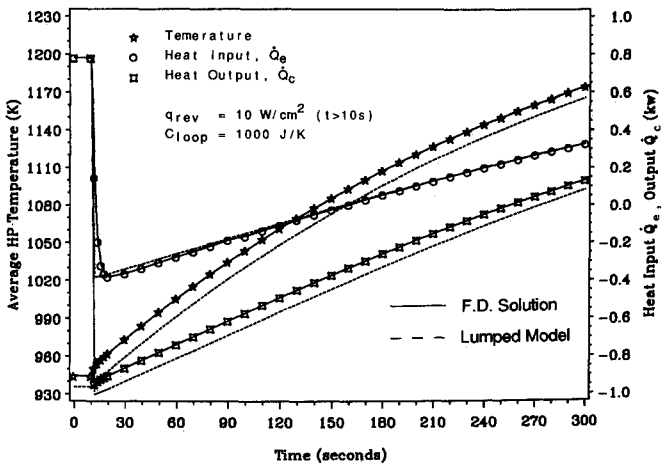

Fig. 7 Comparison of the transient response of the heat pipe without PCM predicted by lumped-heat-capacity model and finite difference method.

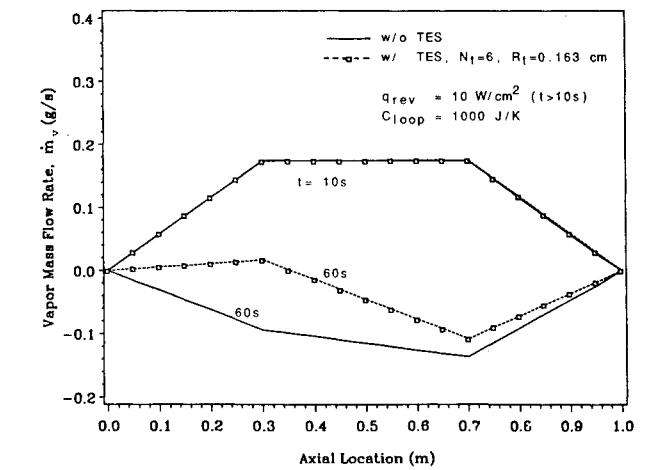

Fig. 8 Vapor mass flow rates of heat pipes.

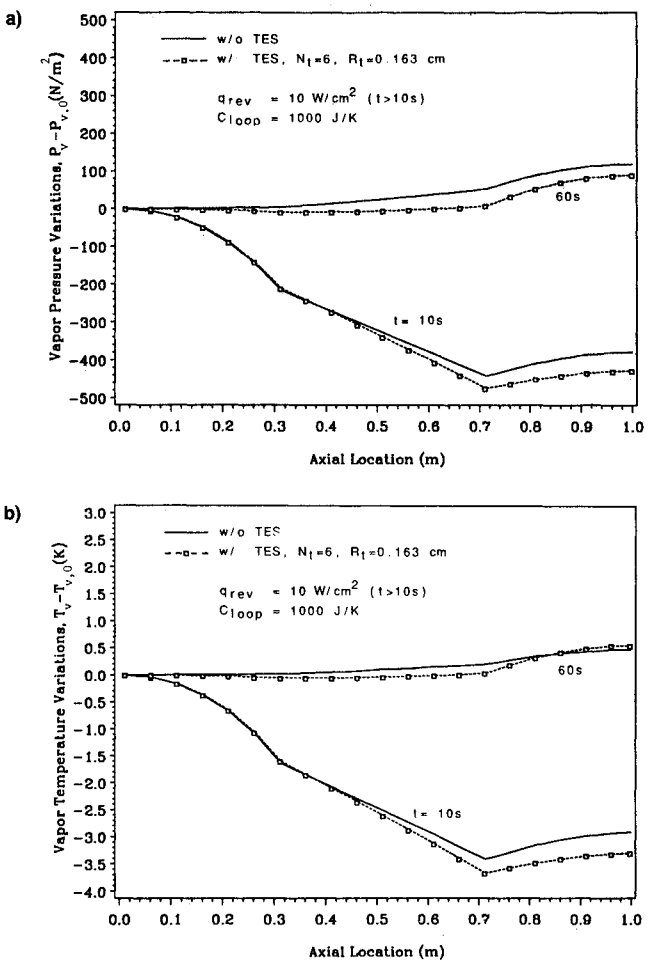

Fig. 9 Axial variation of vapor pressure and temperature.

due to its higher temperature, since the vapor pressure drop is strongly dependent on a heat pipe's operating temperature.[3] For the heat pipe with six small PCM cylinders, the lower pressure drop is a result of higher heat pipe operating temperature, smaller vapor mass flow rate, and shorter vapor flow path due to the two separate vapor flows. We can also see that the axial variation of vapor temperature is very similar to that of vapor pressure.

The transient responses of the heat pipes under a reversed-pulsed heat load applied to the evaporator from $t = 20$ s to $t = 80$ s are shown in Figs. 10 and 11. As we can see from Fig. 10, the temperatures of all three heat pipes respond very rapidly and start to decrease as soon as the reversed-pulsed heat load is removed at $t = 80$ s. The temperature of the heat pipe without PCM decreases very rapidly after the reversed-pulsed heat load is removed. The temperature of each unit with PCM also decreases rapidly immediately after road removal, but the decrease becomes very slow when the PCM reaches its melting point and starts to solidify. The six small PCM cylinders are completely solidified earlier than the single large PCM cylinder. After the PCM cylinders are completely solidified, the temperature of both heat pipes with PCM resumes its decrease, and the heat pipes return to their initial steady-state condition. It takes about 1660 s for the heat pipe with six PCM cylinders and about 2260 s for the one with a single large PCM cylinder to return to their initial steady-state condition after the reversed-pulsed heat load is removed. Figure 11 shows the percentage of PCM melted vs time for the same case illustrated in Fig. 10. We can see that the molten PCM fraction does not respond as rapidly as the heat pipe

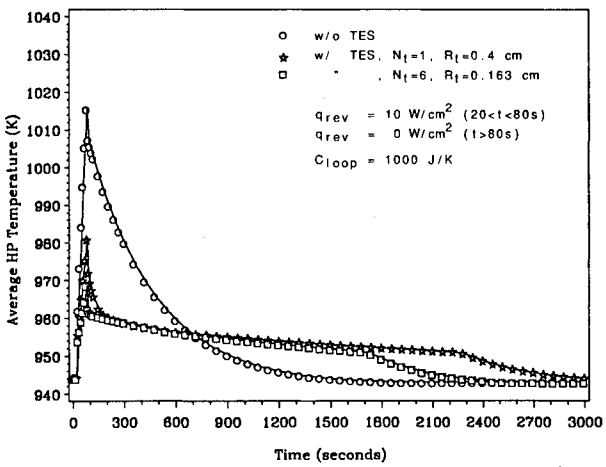

Fig. 10 Transient response of heat pipes under a reversed-pulsed heat load.

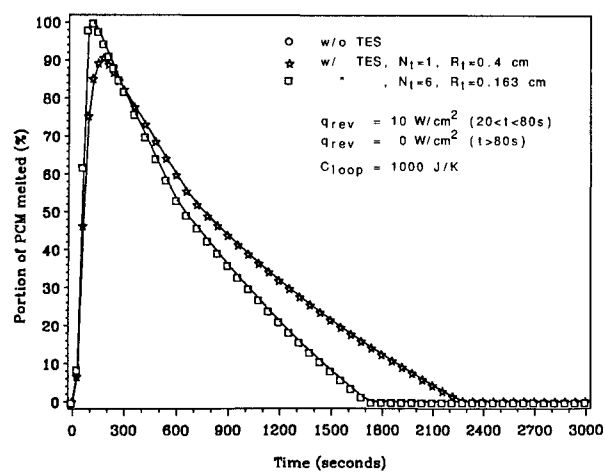

Fig. 11 Portion of PCM melted vs time for a reversed-pulsed heat load.

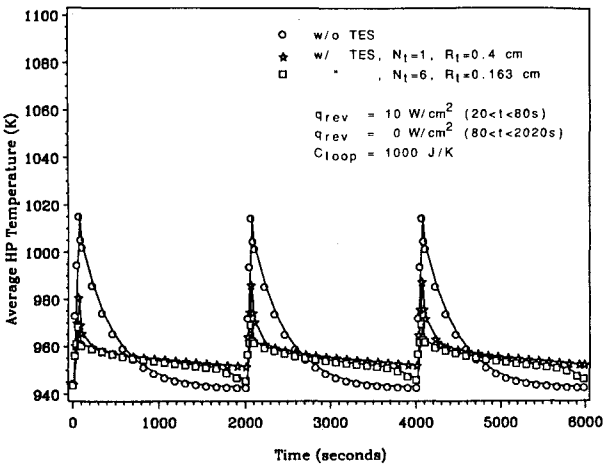

Fig. 12 Transient response of heat pipes under periodic, reversed-pulsed heat load.

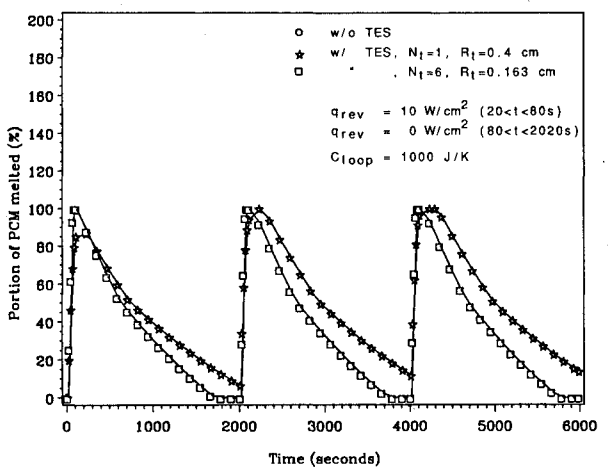

Fig. 13 Portion of PCM melted vs time for periodic, reversed-pulsed heat load.

temperature does. In fact after the reversed-pulsed heat load is removed at $t = 80$ s, 14% more of the six small PCM cylinders and 25% more of the single large PCM cylinder will still be melted before the fusion process stops. It can also be seen that the small PCM cylinder solidifies faster than the large one does.

Figures 12 and 13 show the results of the transient response of the heat pipes with periodic, reversed-pulsed heat loads. The time period of 2000 s and each of the reversed-pulsed heat loads lasts 60 s. The temperature response in each time period is similar to the results shown in Fig. 10. The temperature of the heat pipe without PCM simply oscillates up and down periodically. The temperature of the heat pipe with six small PCM cylinders remains almost constant throughout the whole period due to very efficient melting and solidification. As shown in Fig. 13, the percentage of PCM melted for the heat pipe with six small PCM cylinders does not differ for one cycle to the next. This is because the six small PCM cylinders solidify completely at the end of each time period. The percentage of PCM melted for the heat pipe with one large PCM cylinder continues to increase as the pulse cycles continue, since the single large PCM cylinder does not have enough time to solidify completely at the end of each time period.

Conclusions

In this paper the transient behavior of a heat pipe with TES was modeled using a three-dimensional ADI finite difference method. A PCM encapsulated in cylindrical containers was used as the TES. It was found that the PCM is very effective

in mitigating the adverse effect of reversed-pulsed heat loads applied at the condenser. The six small PCM cylinders are more efficient than the single large PCM cylinder in reducing the heat pipe temperature increase under reversed-pulsed heat loads, and they can also handle periodic, reversed-pulsed heat loads better since they solidify faster. The numerical results also indicated that the heat inputs and outputs of the heat pipes in the cooling system are strongly dependent on the sodium loop heat capacitance. The vapor flow can be reversed or become two separate flows with opposite directions under reversed heat loads. The vapor pressure and temperature drops are also strongly dependent on the operating vapor temperature. Furthermore, it was found that the lumped-heat-capacity model can predict the average heat pipe temperature and the heat flow input/output at the evaporator and condenser very well for the heat pipe without PCM.

Acknowledgments

This research was funded by the Wright Research & Development Center under Contract F33615-87-C-2777. The authors would like to thank Charles D. Sulfredge for his helpful suggestions in reviewing the paper.

References

[1]Tilton, D. E., Chow, L. C., and Mahefkey, E. T., "Transient Response of a Liquid Metal Heat Pipe," *Journal of Thermophysics and Heat Transfer*, Vol. 2, No. 1, 1988, pp. 25–30.

[2]El-Genk, M. S., and Jong, T. S., "An Analysis of the Effect of External Heating on The SP-100 System Radiator Heat Pipes," 23rd Intersociety Energy Conversion Engineering Conference, Denver, CO, July 1988.

[3]Chang, M. J., Chow, L. C., Chang, W. S., and Morgan, M., "Transient Behavior of Axially Grooved Heat Pipe with Thermal Energy Storage," *Journal of Thermophysics and Heat Transfer*, Vol. 6, No. 2, 1992, pp. 364–370.

[4]Chang, M. J., Chow, L. C., and Chang, W. S., "Improved Alternating-Direction-Implicit Method for Solving Transient Three-Dimensional Heat Diffusion Problems," *Numerical Heat Transfer*, Pt. B, Vol. 19, 1991, pp. 69–84.

[5]Bowman, W. J., "Simulated Heat Pipe Vapor Dynamics," Ph.D. Dissertation, Air Force Inst. of Technology, Wright-Patterson AFB, OH, 1987.

[6]Pham, Q. T., "A Fast, Unconditionally Stable Finite-Difference Scheme for Heat Conduction with Phase Change," *International Journal of Heat and Mass Transfer*, Vol. 28, No. 11, 1985, pp. 2079–2084.

[7]Pham, Q. T., "A Note on Some Finite-Difference Methods for Heat Conduction with Phase Change," *Numerical Heat Transfer*, Vol. 11, 1987, pp. 353–359.

[8]Hsiao, J. S., "An Efficient Algorithm for Finite-Difference Analyses of Heat Transfer with Melting and Solidification," *Numerical Heat Transfer*, Vol. 8, 1985, pp. 653–666.

[9]Shapiro, A. H., *The Dynamics and Thermodynamics of Compressible Fluid Flow*, Vol. 1, Ronald Press, New York, 1953, pp. 238–241.